Lasing in metamaterial nanostructures

2010 J. Opt. 12 024013

(http://iopscience.iop.org/2040-8986/12/2/024013)

IOP Publishing Journal of Optics

J. Opt. **12** (2010) 024013 (13pp) doi:10.1088/2040-8978/12/2/024013

Lasing in metamaterial nanostructures

Anan Fang[1], Thomas Koschny[1,2,3] and Costas M Soukoulis[1,2,3]

[1] Ames Laboratory and Department of Physics and Astronomy, Iowa State University, Ames, IA 50011, USA
[2] Institute of Electronic Structure and Laser, FORTH, 71110 Heraklion, Crete, Greece
[3] Department of Materials Science and Technology, University of Crete, 71110 Heraklion, Crete, Greece

E-mail: soukoulis@ameslab.gov

Received 26 June 2009, accepted for publication 9 September 2009
Published 11 January 2010
Online at stacks.iop.org/JOpt/12/024013

Abstract
A self-consistent computational scheme is presented for one-dimensional (1D) and two-dimensional (2D) metamaterial systems with gain incorporated into the nanostructures. The gain is described by a generic four-level system. The loss compensation and the lasing behavior of the metamaterial system with gain are studied. A critical pumping rate exists for compensating the losses of the metamaterial. There exists a wide range of input signals where the composite system behaves linearly. Nonlinearities arise for stronger signals due to gain depletion. The retrieved effective parameters are presented for one layer of gain embedded in two layers of Lorentz dielectric rods and split ring resonators (SRR) with two different gain inclusions: (1) gain is embedded in the gaps only and (2) gain is surrounding the SRR. When the pumping rate increases, there is a critical pumping rate at which the metamaterial system starts lasing.

Keywords: metamaterial, gain material, lasing, loss compensation

(Some figures in this article are in colour only in the electronic version)

1. Introduction

The field of metamaterials [1, 2] is driven by fascinating and far-reaching theoretical visions such as, e.g., perfect lenses [3], invisibility cloaking [4, 5], and enhanced optical nonlinearities [6]. This emerging field has seen spectacular experimental progress in recent years [1, 2]. However, losses are orders of magnitude too large for the envisioned applications. Achieving a reduction by further design optimization appears to be out of reach. However, incorporation of active media (gain) might reduce the losses. The procedure would be to simply inject an electrical current into the active medium, leading to gain and hence to compensation of the losses. However, experiments on such intricate active nanostructures do need guidance from theory via self-consistent calculations (using the semi-classical theory of lasing) for realistic gain materials that can be incorporated into, or close to, dispersive media to reduce the losses at THz or optical frequencies. The need for *self-consistent* calculations stems from the fact that on increasing the gain in the metamaterial, the metamaterial properties change, in turn changing the coupling to the gain medium until a steady state is reached. A specific geometry to overcome the severe loss problem of optical metamaterials and to enable bulk metamaterials with negative magnetic and electric responses and controllable dispersion at optical frequencies is to interleave active, optically pumped gain material layers with the passive metamaterial lattice.

For reference, the best fabricated negative index material operating at around 1.4 μm wavelength [7] has shown a figure of merit, FOM $= -\mathrm{Re}(n)/\mathrm{Im}(n) \approx 3$, where n is the effective refractive index. This experimental result is equivalent to an absolute absorption coefficient of $\alpha = 3 \times 10^4$ cm^{-1}, which is even larger than the absorption of typical direct-gap semiconductors such as, e.g., GaAs (where $\alpha = 10^4$ cm^{-1}). So it looks difficult to compensate the losses with this simple type of analysis, which assumes that the bulk gain coefficient is needed. However, the effective gain coefficient, derived from self-consistent microscopic calculations, is a more appropriate measure of the combined system of metamaterial and gain. Due to pronounced local field enhancement effects in the spatial vicinity of the

dispersive metamaterial, the effective gain coefficient can be substantially larger than its bulk counterpart. While early models [8–12] using simplified gain mechanisms, such as explicitly forcing negative imaginary parts of the local gain material's response function, produce unrealistic strictly linear gain, our self-consistent approach, presented below, allows for determining the range of parameters for which one can realistically expect linear amplification and linear loss compensation in the metamaterial [13]. The approximation in these earlier models can effectively be obtained in our approach by assuming a constant population inversion in the equation (2), i.e., a population inversion given by an 'average field'. To fully understand the coupled metamaterial–gain system, we have to deal with time-dependent wave equations in metamaterial systems by coupling Maxwell's equations with the rate equations of electron populations describing a multi-level gain system in semi-classical theory [14].

This paper aims to apply a detailed computational model to the problem of metamaterials with gain. In section 2, we present the semi-classical theory of lasing and describe in detail the computational approach. In section 3, we verify that our code agrees well with simple soluble models (gain material only). In addition, our code is applied to a 1D superlattice of gain and negative index layers. Next, a 2D problem is considered, which is a square lattice of Lorentz dielectric cylinders with layers of gain material. Finally, a 2D split ring resonator (SRR) with gain material inclusions is considered. Gain can compensate the losses and lasing is achieved in our numerical simulations. In section 4, we present our conclusions.

2. Theoretical and numerical model

The gain atoms are embedded in the host medium and described by a generic four-level system, as shown in figure 1. All quantities including the fields and occupation numbers are tracked at each point in space and take into account the energy exchange between gain atoms and fields, external pumping and non-radiative decays [14]. Electrons are pumped by an external mechanism from the ground state level (N_0) to the third level (N_3). After a short lifetime τ_{32}, they quickly relax into the metastable second level (N_2). The second level (N_2) and the first level (N_1) are called the upper and lower lasing levels, respectively. Electrons can transfer both radiatively (spontaneous and stimulated emissions) and non-radiatively from the upper to the lower lasing level. At last, they transfer quickly and non-radiatively from the first level (N_1) to the ground state level (N_0). The energies of the ground state and the third level are E_0 and E_3. In the optical pumping mechanism, electrons are raised from the ground state level (N_0) to the third level (N_3) by an external electromagnetic wave with a pumping frequency $\omega_b = (E_3 - E_0)/\hbar$, which is chosen to be $4\pi \times 10^{14}$ Hz in our simulations. The local intensity of the pumping EM wave varies with the position and determines the pumping rate at each point. The lifetimes and energies of the upper and lower lasing levels are τ_{21}, E_2 and τ_{10}, E_1, respectively. The center frequency of the radiation is $\omega_a = (E_2 - E_1)/\hbar$, which is chosen to be $2\pi \times 10^{14}$ Hz. The parameters τ_{32}, τ_{21} and τ_{10} are chosen as 5×10^{-14} s, 5×10^{-12} s and 5×10^{-14} s, respectively. The total electron density, $N_0(t=0) = N_0(t)+N_1(t)+N_2(t)+N_3(t) = 5.0\times10^{23}$ m^{-3}.

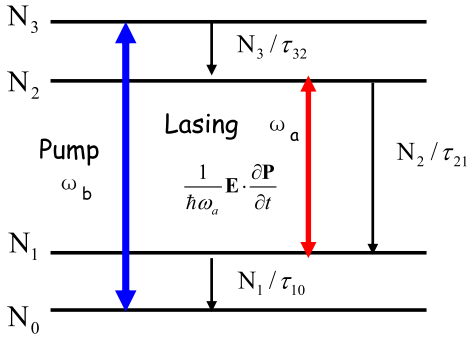

Figure 1. Schematic of the four-level atomic system model.

The time-dependent Maxwell equations are given by

$$\begin{aligned} \nabla \times \mathbf{E} &= -\partial \mathbf{B}/\partial t \\ \nabla \times \mathbf{H} &= \varepsilon\varepsilon_0 \partial \mathbf{E}/\partial t + \partial \mathbf{P}/\partial t, \end{aligned} \tag{1}$$

where $\mathbf{B} = \mu\mu_0\mathbf{H}$, and $\mathbf{P} = \sum_{i=a,b} \mathbf{P}_i$ is the electric polarization density of the gain material. ($\mathbf{P}_a$ is the induced electric polarization density on the atomic transition between the upper (N_2) and lower (N_1) lasing levels, and $\mathbf{P}_b$ is between the ground state level (N_0) and the third level (N_3).) The induced electric polarizations behave as harmonic oscillators and couple to the local $\mathbf{E}$ field, which is propagated by the Maxwell equations. The polarization density $\mathbf{P}_i(\mathbf{r}, t)$ locally obeys the following equation of motion [14]

$$\frac{\partial^2 \mathbf{P}_i(t)}{\partial t^2} + \Gamma_i \frac{\partial \mathbf{P}_i(t)}{\partial t} + \omega_i^2 \mathbf{P}_i(t) = -\sigma_i \Delta N_i(t) \mathbf{E}(t) \quad (i = a, b), \tag{2}$$

where Γ_i is the linewidth of the atomic transition ω_i, σ_i is the coupling strength of $\mathbf{P}_i$ to the electric field, and $\Delta N_a(\mathbf{r}, t) = N_2(\mathbf{r}, t) - N_1(\mathbf{r}, t)$ and $\Delta N_b(\mathbf{r}, t) = N_3(\mathbf{r}, t) - N_0(\mathbf{r}, t)$ are the population inversions that drive the polarizations. In our simulations, Γ_a is chosen to be equal to $2\pi \times 5 \times 10^{12}$ Hz or $2\pi \times 20 \times 10^{12}$ Hz and Γ_b is equal to $2\pi \times 10 \times 10^{12}$ Hz. The values for σ_a and σ_b are taken to be 10^{-4} C^2 kg^{-1} and 5×10^{-6} C^2 kg^{-1}, respectively. From (2), it can be easily derived [14] that the atomic response of gain atoms has a Lorentzian lineshape and is homogeneously broadened. The occupation numbers at each spatial point vary according to the following rate equations,

$$\frac{\partial N_3}{\partial t} = \frac{1}{\hbar\omega_b} \mathbf{E} \cdot \frac{\partial \mathbf{P}_b}{\partial t} - \frac{N_3}{\tau_{32}}, \tag{3a}$$

$$\frac{\partial N_2}{\partial t} = \frac{N_3}{\tau_{32}} + \frac{1}{\hbar\omega_a} \mathbf{E} \cdot \frac{\partial \mathbf{P}_a}{\partial t} - \frac{N_2}{\tau_{21}}, \tag{3b}$$

$$\frac{\partial N_1}{\partial t} = \frac{N_2}{\tau_{21}} - \frac{1}{\hbar\omega_a} \mathbf{E} \cdot \frac{\partial \mathbf{P}_a}{\partial t} - \frac{N_1}{\tau_{10}}, \tag{3c}$$

$$\frac{\partial N_0}{\partial t} = -\frac{1}{\hbar\omega_b} \mathbf{E} \cdot \frac{\partial \mathbf{P}_b}{\partial t} + \frac{N_1}{\tau_{10}}, \tag{3d}$$

where $\frac{1}{\hbar\omega_i} \mathbf{E} \cdot \frac{\partial \mathbf{P}_i}{\partial t}$ $(i = a, b)$ is the induced radiation rate or excitation rate, depending on its sign.

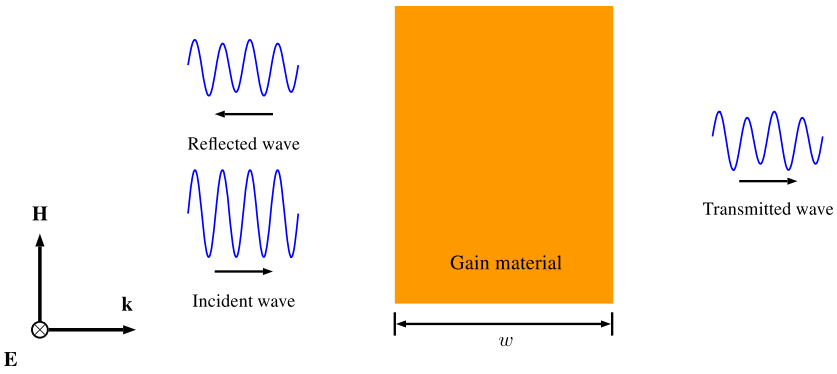

Figure 2. Schematic of gain material slab (shown in orange). The slab width w takes different values in the cases we have examined.

Instead of using an external EM wave to optically pump electrons from the ground state level (N_0) to the third level (N_3), we can simplify this process in (3*a*) and (3*d*) by pumping electrons with a homogeneous pumping rate Γ_{pump}, which is proportional to the optical pumping intensity in an experiment. This simplification is valid only if the gain slab is thin and the gain of the laser is low, because the real pumping rate depends on the local optical intensity and should be a function of position. We will discuss this in more detail in section 3.1. Based on this simplification, we can write the rate equations as follows,

$$\frac{\partial N_3}{\partial t} = \Gamma_{\text{pump}} N_0 - \frac{N_3}{\tau_{32}}, \tag{4a}$$

$$\frac{\partial N_2}{\partial t} = \frac{N_3}{\tau_{32}} + \frac{1}{\hbar\omega_a}\mathbf{E}\cdot\frac{\partial \mathbf{P}_a}{\partial t} - \frac{N_2}{\tau_{21}}, \tag{4b}$$

$$\frac{\partial N_1}{\partial t} = \frac{N_2}{\tau_{21}} - \frac{1}{\hbar\omega_a}\mathbf{E}\cdot\frac{\partial \mathbf{P}_a}{\partial t} - \frac{N_1}{\tau_{10}}, \tag{4c}$$

$$\frac{\partial N_0}{\partial t} = \frac{N_1}{\tau_{10}} - \Gamma_{\text{pump}} N_0. \tag{4d}$$

Correspondingly, we only need to consider the electric polarization density $\mathbf{P}_a(\mathbf{r}, t)$ on the atomic transition between N_2 and N_1 in (1) and (2).

In order to solve the behavior of the gain materials in the electromagnetic fields numerically, the finite-difference time-domain (FDTD) method is utilized [15–19]. At the left and right ends of the computational space, perfect matched layers (PML) are used to impose the absorbing boundary condition (ABC). In the FDTD calculations, both the space and time are discretized into small steps compared to the characteristic space and time periods. In our simulations, presented below, the discrete time and space steps are chosen to be $\Delta t = 1.67 \times 10^{-17}$ s and $\Delta x = 1.0 \times 10^{-8}$ m in sections 3.1 and 3.2, $\Delta t = 8.33 \times 10^{-18}$ s and $\Delta x = 5.0 \times 10^{-9}$ m in section 3.3, and $\Delta t = 8.33 \times 10^{-19}$ s and $\Delta x = 1.0 \times 10^{-9}$ m in section 3.4. The initial condition is that all electrons are in the ground state and all electric, magnetic and polarization fields are zero. Then the electrons are pumped from N_0 to N_3 optically or with a homogeneous pumping rate Γ_{pump}. The system begins to evolve according to the equations above. The FDTD update algorithm is given in the appendix.

3. Examples for metamaterials incorporated with gain

3.1. Gain material only

To understand the lasing behavior of the gain material, we first study a gain material slab surrounded by vacuum (shown in figure 2). We generate a continuous wave (CW) at the frequency ω_b (200 THz) and let it propagate through the gain slab, and then we calculate the reflected and transmitted waves and implement Fourier transforms to see if there is lasing and how much power is emitted around 100 THz—the emission frequency ω_a between N_1 and N_2. First we start with a very low input power P_{in} for the incident CW wave, here no lasing happens, then we increase the input power until it reaches the lasing threshold, for which the system starts to lase and we can see a small peak at the emission frequency 100 THz in the Fourier transforms of the reflected and transmitted waves, i.e., low power emitted around the emission frequency ω_a. If we keep increasing the input power, the peak will get higher and the emitted power will get larger. Figure 3 shows the transmitted waves and their corresponding Fourier transforms for three different input powers at the gain slab $w = 100$ nm. We can see there is no lasing (figure 3(a)) when the input power is low ($P_{\text{in}} = 79.6$ W mm^{-2}) and there is only one peak for the pumping frequency in its Fourier transform (figure 3(b)). When the input power $P_{\text{in}} = 90.7$ W mm^{-2}, the system starts lasing (figure 3(c)) and a small peak appears at the frequency 100 THz (figure 3(d)). If we increase the input power to a higher value $P_{\text{in}} = 120.6$ W mm^{-2}, the lasing gets stronger (figure 3(e)) and the peak for the emission frequency gets higher (figure 3(f)), i.e., more power emitted around the emission frequency ω_a. We have calculated the emitted power at the emission frequency ω_a versus the input power at the pumping frequency ω_b for the same gain slab system. As shown in figure 4, we can see that there is a sharp rise in the emission around $P_{\text{in}} \approx 90.7$ W mm^{-2}, which corresponds to the lasing threshold for this system. Below the threshold, there is no lasing.

We also notice that the lasing time (the time when the system starts lasing) varies according to the input power. Figure 5 shows the detailed results for the lasing time versus the input power with the slab widths $w = 100, 250$ and 500 nm. We can see the lasing time decreases as the input

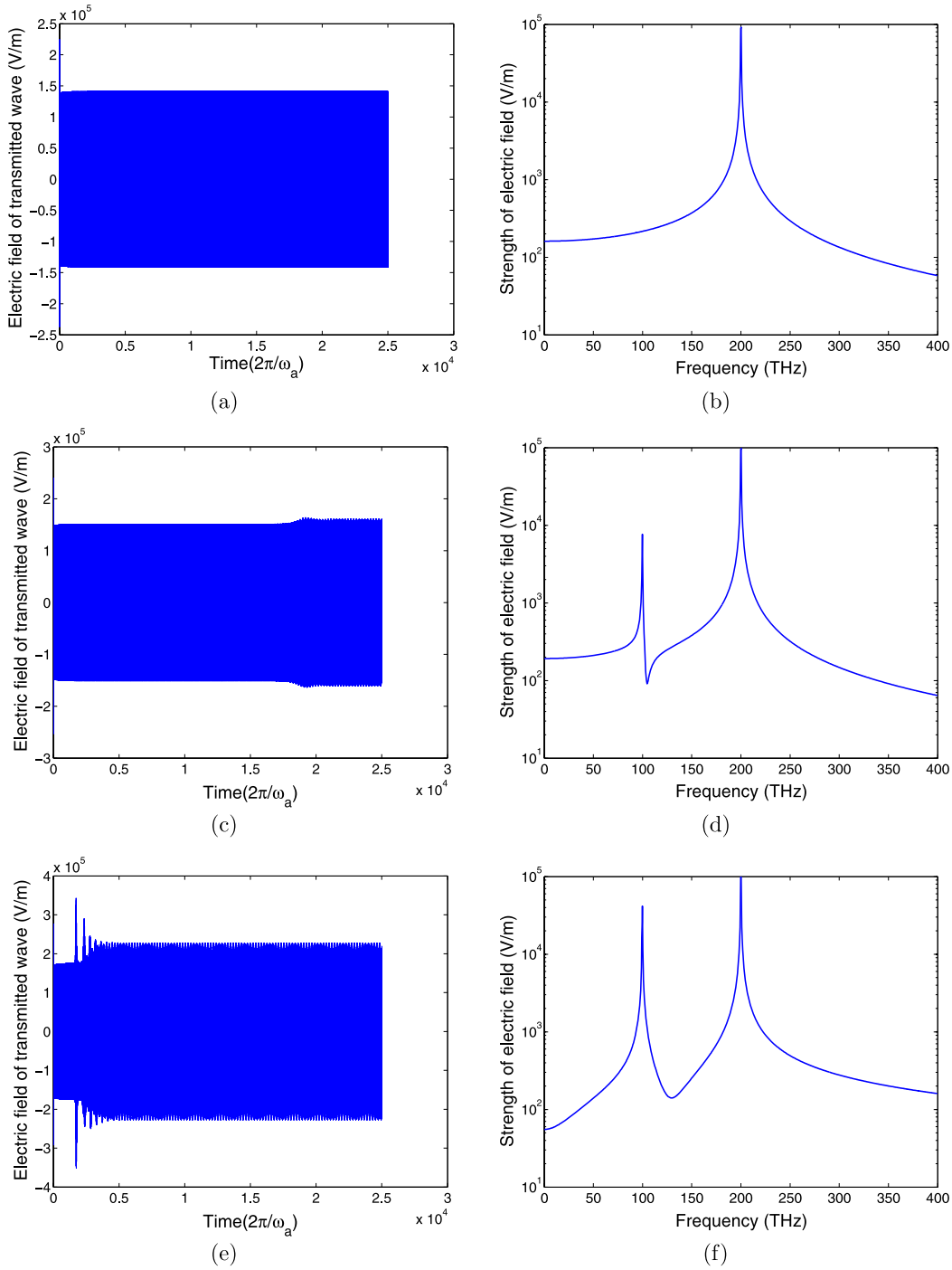

Figure 3. The transmitted waves and their corresponding Fourier transforms for different input powers. (a), (c) and (e) are the transmitted waves for input power $P_{\text{in}} = 79.6,\ 90.7$ and 120.6 W mm^{-2}, respectively. (b), (d) and (f) are same as (a), (c) and (e), respectively, but are the Fourier transforms of the transmitted waves. The gain slab width $w = 100$ nm and the bandwidth Γ_a of the atomic transition between N_1 and N_2 is 5 THz.

power increases because the system pumps the electrons at a higher rate from the ground state level to higher levels and then reaches the population inversion between N_1 and N_2 in a shorter time. For a fixed input power, one can see the lasing time decreases as the gain slab width gets larger. This occurs because more input energy is absorbed and then converted to lasing by the wider gain slab.

As the input wave propagates inside the gain slab, it will decay due to the absorption from the gain material at the pumping frequency ω_b (see figure 6). Thus the pumping rate, which is determined by the local input optical intensity, is inhomogeneous inside the gain slab. However, for a thin gain material layer, the electric field of the input wave can be approximately treated as homogeneous, thus we can

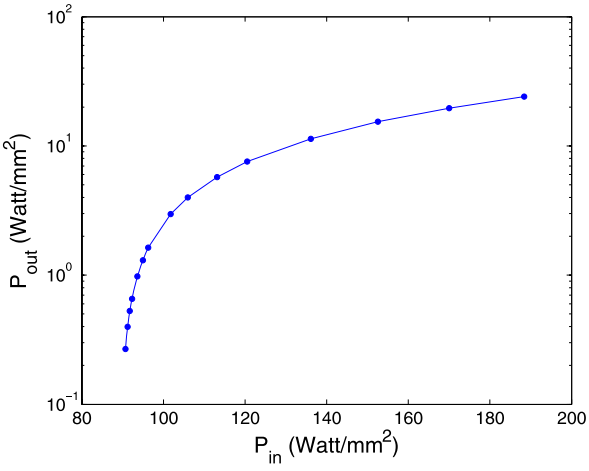

Figure 4. The powers emitted at the emission frequency $\omega = \omega_a$ (100 THz) for different input powers at the pumping frequency $\omega = \omega_b$ (200 THz). All parameters of this system are the same as figure 3.

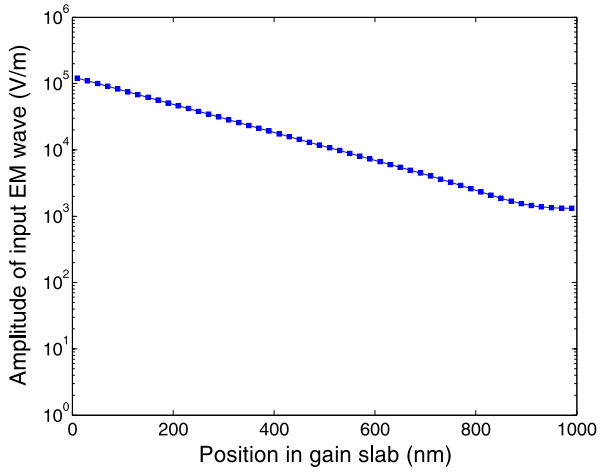

Figure 6. The amplitude of the input EM wave inside the gain slab as a function of the position. The gain slab width $w = 1000$ nm and the input power $P_{\text{in}} = 92.3$ W mm^{-2}. All other parameters are the same as figure 3.

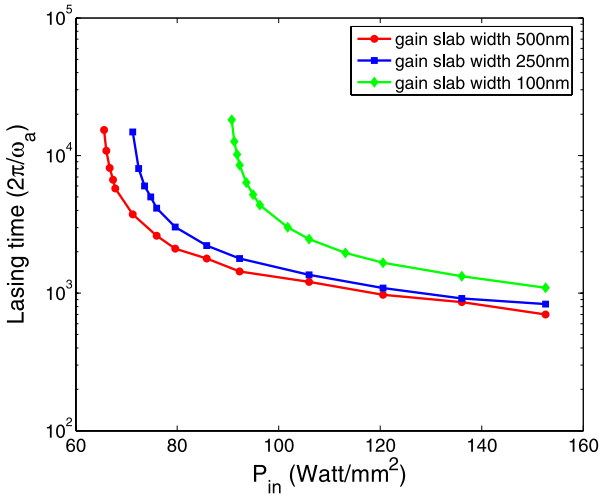

Figure 5. The lasing times for different input powers at the pumping frequency ω_b (200 THz). The gain slab width $w = 100$ nm, 250 nm and 500 nm, respectively. All other parameters are the same as figure 3.

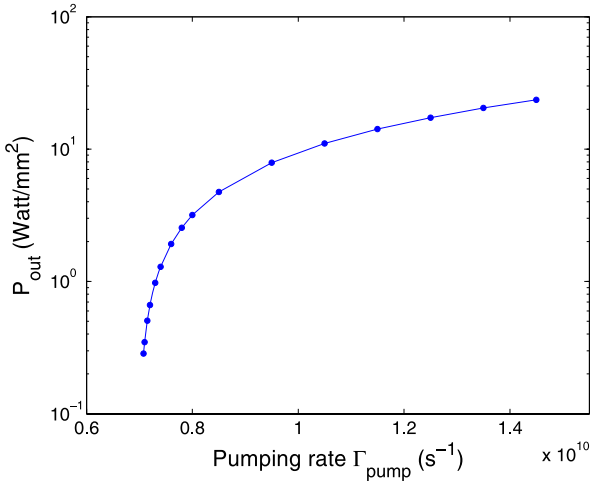

Figure 7. The powers emitted at the emission frequency $\omega = \omega_a$ (100 THz) for different pumping rates. The gain slab width $w = 100$ nm and the bandwidth of the atomic transition between N_1 and N_2 is 5 THz.

simplify the pumping process between N_0 and N_3 by using a homogeneous pumping rate Γ_{pump}. For a very thin gain slab $w = 100$ nm, simulations are done with a homogeneous pumping rate and the results for the power emitted around the emission frequency ω_a versus the pumping rate are plotted in figure 7. Comparing this with figure 4, where the electrons are optically pumped, we can see they are very similar. For a fixed output power, such as $P_{\text{out}} = 7.56$ W mm^{-2}, we can find the corresponding input power $P_{\text{in}} = 120.6$ W mm^{-2} in figure 4 and the corresponding pumping rate $\Gamma_{\text{pump}} = 9.3 \times 10^9$ s^{-1} in figure 7. Then we do simulations for optical pumping case with the input power $P_{\text{in}} = 120.6$ W mm^{-2} and for the homogeneous pumping rate case with the pumping rate $\Gamma_{\text{pump}} = 9.3 \times 10^9$ s^{-1}. The graphs of the occupation numbers as a function of time are plotted in figure 8 for both cases. One can see that they are almost the same. This verifies that the homogeneous pumping rate simplification is valid for a thin gain slab. In our following simulations we will use this simplification because the gain slab widths in our structures are very thin ($w \leqslant 50$ nm).

3.2. Negative index material (NIM) embedded in layers of gain

As the first simple model system, we will discuss a one-dimensional metamaterial system which consists of layers of negative index material (NIM) and gain material, as shown in figure 9, to see if we can compensate the losses of the metamaterials associated with the NIMs by the amplification provided by the gain material layers and how the system starts lasing. We first let a narrow band Gaussian pulse of a given amplitude go through the metamaterial without gain,

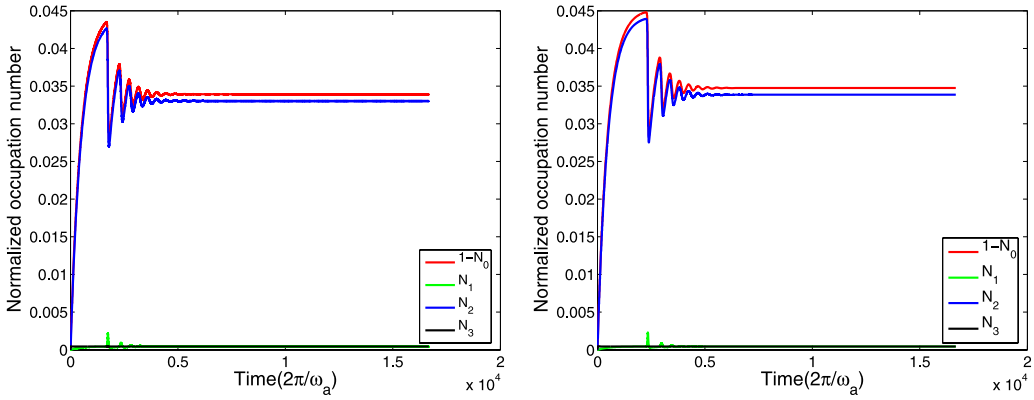

Figure 8. The normalized occupation numbers as a function of time. The gain slab width $w = 100$ nm and the gain bandwidth of the atomic transition between N_1 and N_2 is 5 THz. (a) The electrons are optically pumped by an input EM wave with input power $P_{\text{in}} = 120.6\ \text{W mm}^{-2}$ and (b) the electrons are pumped with a homogeneous pumping rate $\Gamma_{\text{pump}} = 9.3 \times 10^9\ \text{s}^{-1}$. Occupation numbers N_0, N_1, N_2 and N_3 are normalized by the total electron density N_i ($N_i = N_0(t = 0) = 5.0 \times 10^{23}\ \text{m}^{-3}$).

Figure 9. The negative index material (blue) embedded in layers of gain material (orange). The number of layers, the permittivity and permeability of NIM take different values for the different cases we have examined. The width for both NIM and gain material is $w = 50$ nm. The gain bandwidth is 5 THz.

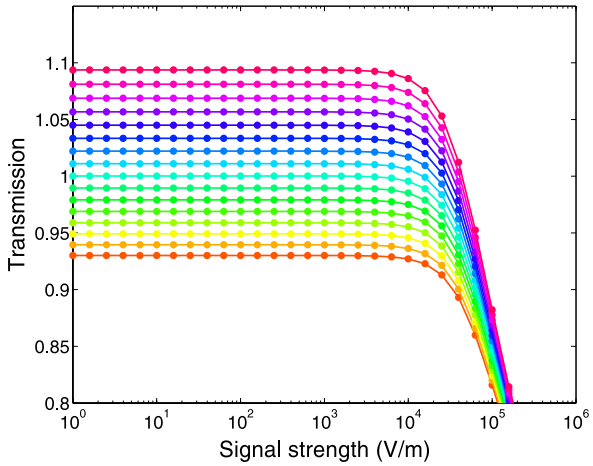

Figure 10. The transmission versus signal amplitude for the loss-compensated metamaterial of a three-layer system (NIM–gain material–NIM) with a gain bandwidth of 5 THz, for different pumping rates Γ_{pump}. Γ_{pump} is increased from $4.0 \times 10^9\ \text{s}^{-1}$ (lowest) to $5.5 \times 10^9\ \text{s}^{-1}$ (highest) in steps of $1.0 \times 10^8\ \text{s}^{-1}$. The material parameters for NIM are $\varepsilon = \mu = -1 + 2\,\text{i}$. The metamaterial response is linear over a very wide range. When the loss-compensated transmission reaches exactly unity, the pumping rate $\Gamma_{\text{pump}} = 4.70 \times 10^9\ \text{s}^{-1}$; this is called the critical pumping rate. For incident fields stronger than $10^4\ \text{V m}^{-1}$ the metamaterial behaves nonlinearly.

and we calculate the transmitted signal emerging from the metamaterial system, which also has a Gaussian profile but its amplitude is much smaller than that of the incident pulse due to the losses of NIM layers. Then we introduce the gain into the system and start increasing the pumping rate.

The amplitude of the transmitted signal gets larger and we can find a critical pumping rate, for which the transmitted pulse is of the same amplitude as the incident one. Since the gain material itself is nonlinear, we increase the amplitude of the incident Gaussian pulse for a fixed pumping rate to see how high we can go in the strength of the incident electric field and still have full compensation of the losses, i.e., the transmitted signal equals the incident signal, independent of the signal strength. In this region we have compensated loss and still have a linear response of the metamaterial. The shape of the transmitted signal is only affected by the dispersion and is not dependent on the signal strength. For a three-layer system (NIM–gain material–NIM), we have calculated the transmission versus the strength of the electric field of the incident signal for several pumping rates close to the critical pumping rate $\Gamma_{\text{pump}} = 4.70 \times 10^9\ \text{s}^{-1}$, as shown in figure 10. We find it has a linear response within a very broad range up to incident electric field of $10^3\ \text{V m}^{-1}$. If we use 19 layers of figure 9, the critical pumping rate is $1.98 \times 10^9\ \text{s}^{-1}$, which is even smaller than half of the three-layer case, and the linear regime becomes narrower and drops faster than the three-layer case for a higher strength of incident electric field (shown in figure 11). To include the nonlinearity of the gain material for a strong incident signal, it is necessary to do a self-consistent calculation using the FDTD method.

As an example, we have also studied the three-layer system with different losses, to see how much Γ_{pump} we need to compensate the losses. Figure 12 shows there exists a linear relation between the critical pumping rate and the imaginary part of the refractive index n of NIMs.

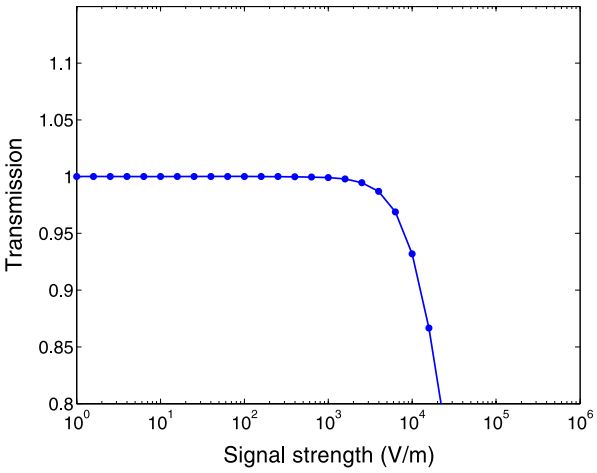

Figure 11. The transmission versus signal amplitude for the loss-compensated metamaterial of figure 9 with a gain bandwidth of 5 THz at the critical pumping rate $\Gamma_{\text{pump}} = 1.98 \times 10^9\ \text{s}^{-1}$. The material parameters for the NIM are same as figure 10. For incident fields stronger than $10^3\ \text{V m}^{-1}$ this metamaterial becomes nonlinear.

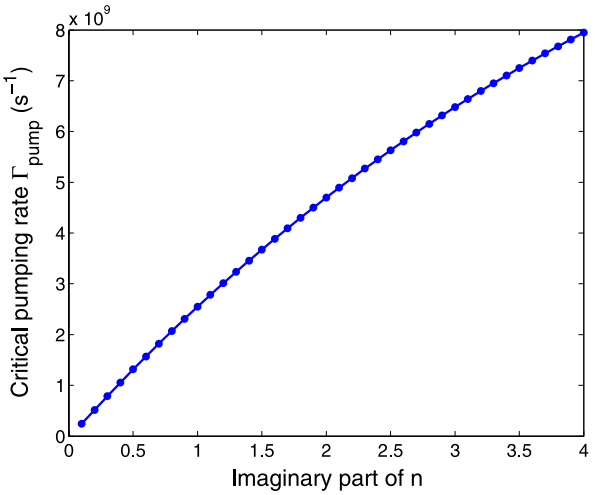

Figure 12. The critical pumping rates for different imaginary parts of the refractive index n of NIMs. The structure is a three-layer system (NIM—gain material—NIM) and $\varepsilon = \mu$ for NIMs.

We have also numerically calculated the susceptibilities of the gain material to see if it really has a Lorentzian lineshape. We first let a Gaussian pulse of a given amplitude ($10\ \text{V m}^{-1}$) propagate through the metamaterial system and calculate the time-domain electric polarization $\mathbf{P}(\mathbf{r}, t)$ and the local electric field $\mathbf{E}(\mathbf{r}, t)$. Then we implement the Fourier transforms to obtain the frequency-domain polarization and electric fields and calculate the frequency-dependent susceptibility by using the equation $\chi'(\omega) + \mathrm{i}\chi''(\omega) = P(\omega)/\varepsilon_0 E(\omega)$. Simulations are done for both 3 and 19 layers and results are compared with the analytic results calculated using the equations [14] $\chi' = -\chi_0''\Delta x/(1 + \Delta x^2)$ and $\chi'' = \chi_0''/(1 + \Delta x^2)$ with $\Delta x = 2(\omega - \omega_a)/\Gamma_a$ and $\chi_0'' = -\sigma_a \Delta N/(\varepsilon_0 \omega_a \Gamma_a)$, where $\Delta N = N_2 - N_1$. As shown in figure 13, we find that the numerical susceptibilities are the same as the analytic ones and they do have a Lorentzian lineshape.

To understand the lasing behavior of the metamaterial system, we increase the pumping rate to provide more gain from the gain material. We found the amplification of the incident signal gets larger and at last the system starts lasing until the pumping rate reaches a certain high value. Figure 14(a) shows the lasing behavior at the pumping rate $\Gamma_{\text{pump}} = 1.5 \times 10^{10}\ \text{s}^{-1}$ and where a peak appears at the emission frequency 100 THz in the corresponding Fourier transform (figure 14(b)).

If we use real metal layers instead of negative index materials, we cannot compensate the losses of the metals. The reason is that the permittivity ε for metals is large and negative and we will have large reflections due to the impedance mismatch.

3.3. One layer of gain material embedded in a square lattice of Lorentz dielectric cylinders

In section 3.2, we simply force the permittivity and the permeability of the metamaterial to be negative to have an unrealistic negative index material. In this section, we

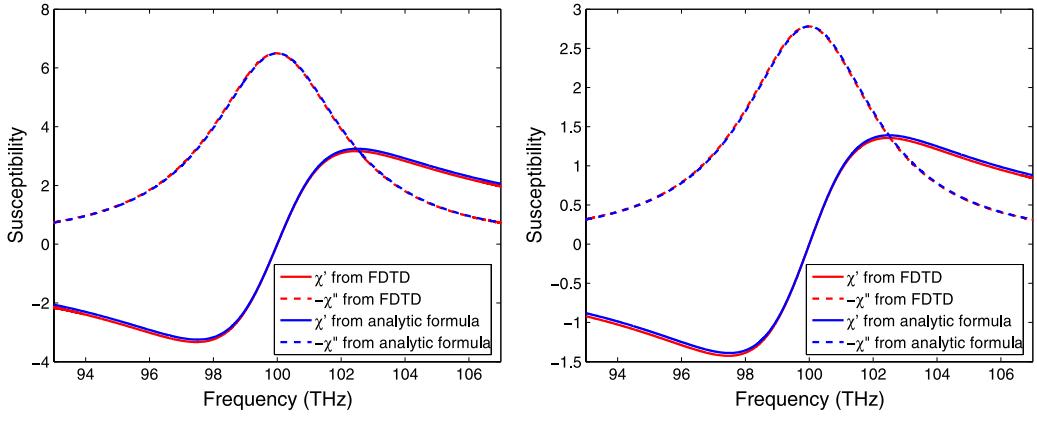

Figure 13. The numerical and analytical results for the susceptibilities of gain materials as a function of frequency. (a) A three-layer system (NIM—gain material—NIM) at the critical pumping rate $\Gamma_{\text{pump}} = 4.7 \times 10^9\ \text{s}^{-1}$. (b) A 19-layer system of figure 9 at the critical pumping rate $\Gamma_{\text{pump}} = 1.98 \times 10^9\ \text{s}^{-1}$.

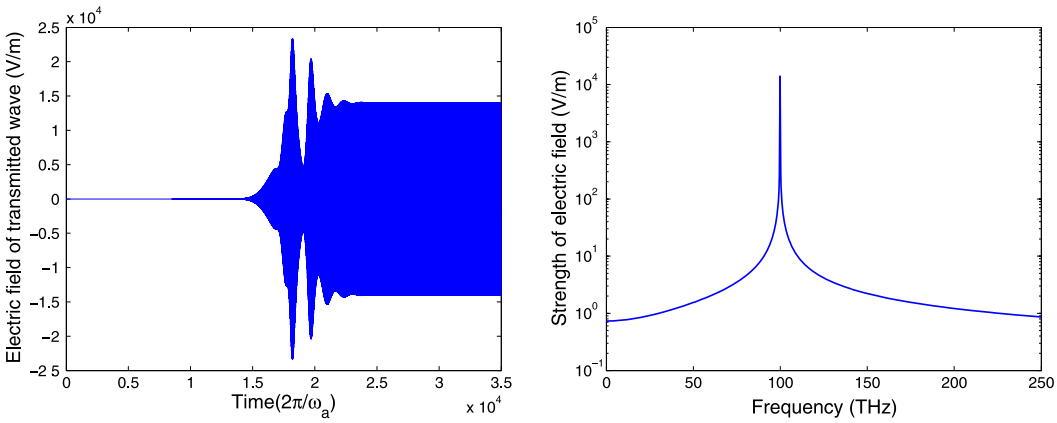

Figure 14. (a) The time-dependent electric field of the transmitted wave for a three-layer system (NIM—gain material—NIM) and (b) the corresponding Fourier transform in frequency domain for the lasing in (a). The pumping rate $\Gamma_{\text{pump}} = 1.5 \times 10^{10}\ \text{s}^{-1}$.

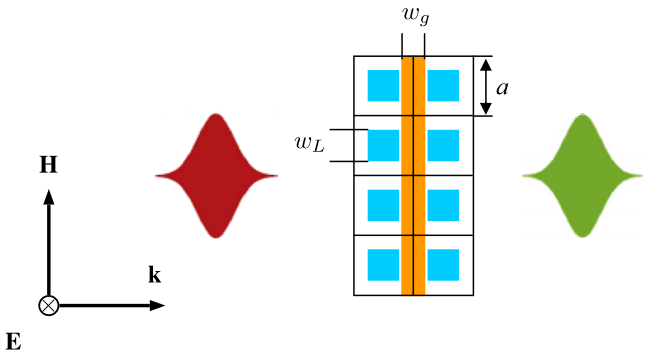

Figure 15. One layer of gain material (orange) embedded in a square lattice of dielectric square cylinders (blue) that have a Lorentz behavior. The dielectric constant of the cylinders is given by $\varepsilon = 1 + \omega_p^2/(\omega_p^2 - 2i\omega\gamma - \omega^2)$, where the resonance frequency $f_p = \omega_p/2\pi = 100$ THz and $\gamma = 2\pi f$, and f takes different values in the cases we have examined. The dimensions are $a = 80$ nm, $w_{\text{L}} = 40$ nm, and $w_{\text{g}} = 30$ nm.

consider a two-dimensional (2D) metamaterial system (shown in figure 15) which consists of one layer of gain material and two layers of dielectric wires that have a Lorentz-type resonant electric response to emulate the resonant elements in a realistic metamaterial, such as cut-wires.

We first study the three-layer system of figure 15 with the full width at half maximum (FWHM) 5 THz for the Lorentz dielectric (i.e., $f = 2.5$ THz) and 20 THz for gain. The transmission, T, the reflection, R, and the absorption, $A = 1 - T - R$, as a function of frequency for the system are obtained in the propagation direction. With the introduction of gain, the absorption at the resonance frequency of 100 THz decreases and reaches 0 at a certain pumping rate. So the gain compensates the losses. If we continue increasing the gain, i.e., the pumping rate, the system gets overcompensated and the absorption becomes negative. To see how the losses of the emulated resonators get compensated by the gain, we exploit the usual retrieval procedure based on inverting the scattering amplitudes [20] to obtain the effective permittivities ε without gain and with gain. Figures 16(a), (c) and (e) show the retrieved results for the real and the imaginary parts of the effective permittivities ε of the system for the below compensation, loss-compensated, and overcompensated cases, respectively, together with the effective permittivity without gain. The retrieved results for ε without gain have an exactly Lorentzian shape but the amplitude of the real and the imaginary parts of ε is a factor of 4 less than the Lorentz formula for the square cylinders. This is due to the filling ratio of the square cylinders in the unit cell. Due to the loss compensation from the gain material, one can see the imaginary part of the effective permittivity gets lower as the gain increases. Below compensation, its value at the resonance frequency of 100 THz is positive, while it is zero and negative for the loss-compensated and overcompensated cases, respectively. Notice that we have $\text{Re}(\varepsilon) \approx 2$ with $\text{Im}(\varepsilon) \approx 0$ at 98 THz and $\text{Re}(\varepsilon) \approx -1$ with $\text{Im}(\varepsilon) \approx 0$ at 101 THz for the below compensation case (figure 16(a)). For the loss-compensated case (figure 16(c)), we have $\text{Re}(\varepsilon) \approx 1$ with $\text{Im}(\varepsilon) \approx 0$ at the resonance frequency 100 THz, which is exactly the same as a vacuum and makes no sense for us. For the overcompensated case (figure 16(e)), the imaginary part of the effective permittivity ε is negative for the whole frequency range.

Secondly, we study the three-layer system with the FWHM of gain smaller than the Lorentz dielectric, where the bandwidths for gain and Lorentz dielectric are 5 THz and 20 THz (i.e., $f = 10$ THz), respectively. The introduction of gain develops a peak at the resonance frequency of 100 THz for the transmission, while the absorption has a dip. The retrieved results for the real and the imaginary parts of the effective permittivities ε without gain and with gain are plotted in figures 16(b), (d) and (f) for the three different cases discussed above. Similar to the first case we examined, where the loss bandwidth is smaller than the gain, the imaginary part of the effective permittivity ε gets smaller due to the gain. The difference is that we get interesting results for the overcompensated case instead of the below compensation case, where we have $\text{Re}(\varepsilon) \approx 0$ with $\text{Im}(\varepsilon) \approx 0$ at 97 THz and $\text{Re}(\varepsilon) \approx 2.1$ with $\text{Im}(\varepsilon) \approx 0$ at 103 THz.

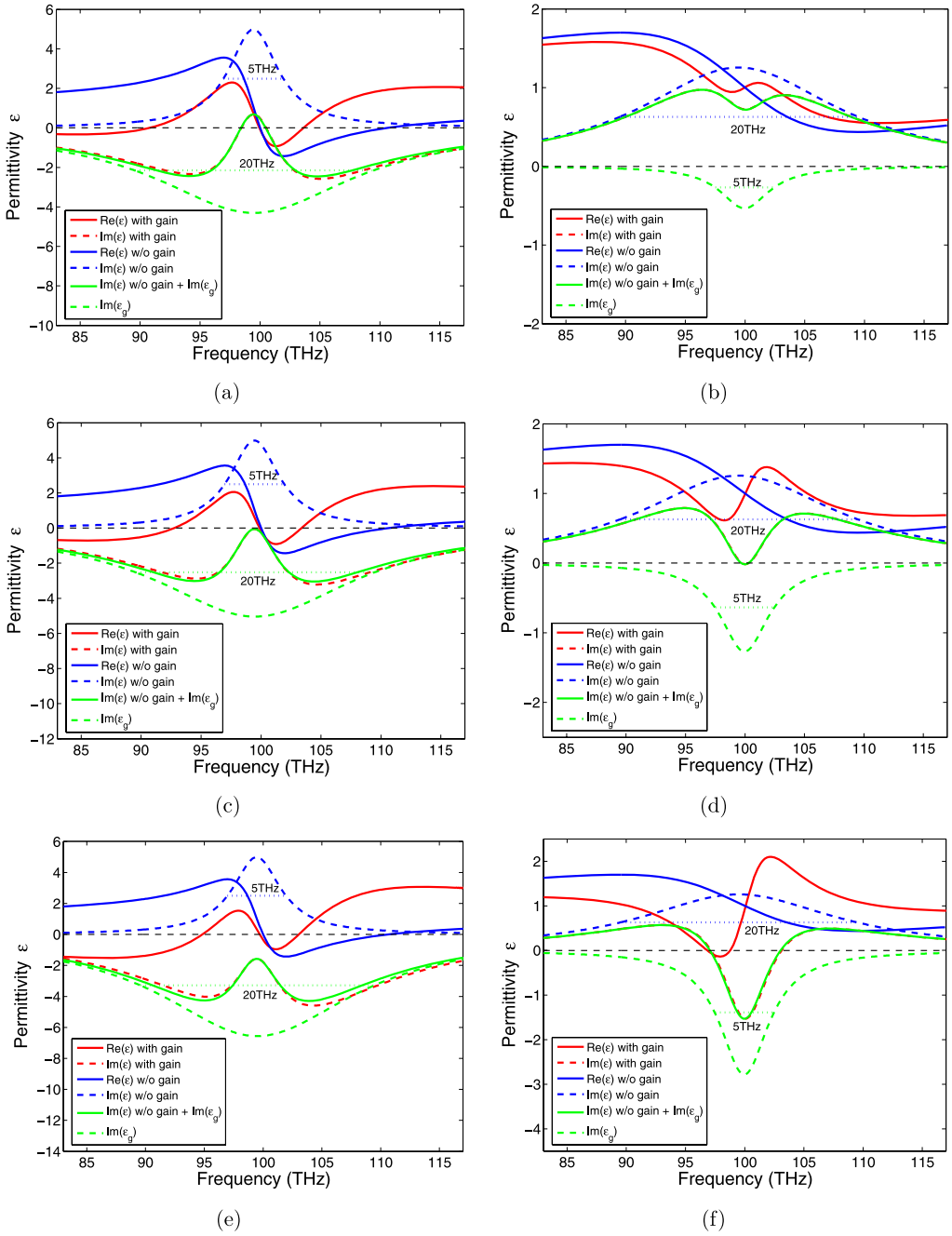

Figure 16. (a) The retrieved results for the real and the imaginary parts of the effective permittivity ε with gain and without gain. Below compensation, $t = 0.89$; gain and Lorentz bandwidths are 20 THz and 5 THz, respectively. (c) and (e) are same as (a), but for the loss-compensated case ($t = 1$) and the overcompensated case ($t = 1.34$), respectively. (b), (d) and (f) are same as (a), (c) and (e), respectively, except with the gain bandwidth 5 THz and Lorentz bandwidth 20 THz.

So for both the two systems, one can obtain a lossless metamaterial with positive or negative Re(ε), either below compensation or over compensation. In figure 16 we have also plotted the sum of Im(ε) without gain and the imaginary part of ε_g, the dielectric function of the gain material. One can see the imaginary part of ε of our total system with gain is equal to the sum of Im(ε) and Im(ε_g). This is unexpected because there is no coupling between the Lorentz dielectric and the gain. This is indeed true for the 2D Lorentz dielectric cylinders, because they have a continuous shape like a solenoid and the gain material slabs have zero depolarization field. Different from finite length wires (hence a three-dimensional (3D) problem) where the dipole interactions between Lorentz wires and gain material are dominated by the near field $O(1/r^3)$, the interaction for infinite length wires is only via the propagating field $O(\omega \ln |kr|)$, and much weaker. That is why the Lorentz wires and the gain material are approximately independent in our 2D simulations. So there is a need for a true 3D simulation to solve this problem and obtain different behaviors. However, the 3D simulation is computationally excessively demanding.

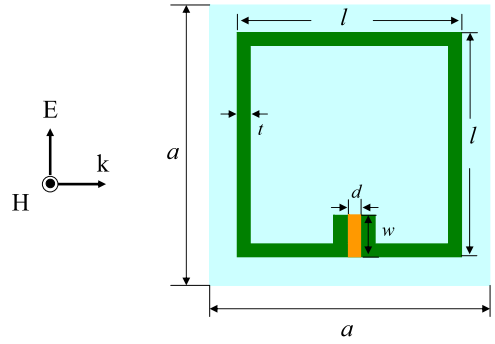

Figure 17. Geometry for a unit cell of the square SRR system with gain embedded in the gap (orange). The dimensions are $a = 100$ nm, $l = 80$ nm, $t = 5$ nm, $d = 5$ nm and $w = 15$ nm.

Like the layered system in section 3.2, if we keep increasing the pumping rate, i.e., the gain, at last both of the two systems will have lasing. For example, when the pumping rate reaches $\Gamma_{\text{pump}} = 3.2 \times 10^{10}$ s^{-1}, the three-layer system with gain bandwidth 5 THz and Lorentz bandwidth 20 THz starts lasing—the system itself has a coherent self-sustained steady output.

3.4. 2D split ring resonators (SRRs) with gain material inclusions

To avoid the decoupling problem in section 3.3 and still limit our simulations in a 2D model, we consider a 2D split ring resonator (SRR) as a more realistic and also more relevant model, where the relevant polarization is across the finite SRR gap and therefore the coupling to the gain material is dipole like. In figure 17, we show the geometry for the unit cell of the SRR system with the gain material embedded in the gap. The dimensions of the SRR are chosen such that the magnetic resonance frequency of the SRR overlaps with the emission frequency (100 THz) of the gain material. Due to the strong electric field inside the gap, there will be strong coupling between the SRR and the gain material. We also want to see if the losses of the magnetic response can be compensated by the electric gain.

Simulations are done for one layer of the square SRR with a gain bandwidth of 20 THz. Figure 18(a) shows the retrieved results for the real and the imaginary parts of the effective permeability μ, with gain (pumping rate $\Gamma_{\text{pump}} = 1.0 \times 10^9$ s^{-1}) and without gain. One can see that with the introduction of gain, the gain undamps the magnetic resonance of the SRR and the weak and broad resonant effective permeability μ of the lossy SRR becomes strong and narrow. The FWHM with gain is 2.61 THz, while the FWHM without gain is 5.85 THz, which is more than twice as large as the former. Notice that in the off-resonance range in figure 18(a), we obtain an effective permeability μ with a smaller imaginary part with the introduction of the gain, which means the magnetic loss is compensated by the electric gain. Figure 18(b) shows the retrieved results for the real and the imaginary parts of the corresponding effective index of refraction n, with and without gain. Note that for a lossless SRR, n is purely real away from the resonance except in a small band above the resonance where it is purely imaginary due to the negative μ. At a frequency of 96 THz, slightly below the resonance (figure 18(b)), the imaginary parts of the index of refraction n without and with gain are 1.36 and 0.754 respectively. Thus we find the effective extinction coefficient without gain is $\alpha = (\omega/c)\,\text{Im}(n) \approx 2.74 \times 10^4$ cm^{-1} and with gain is $\alpha \approx 1.52 \times 10^4$ cm^{-1}. Hence the effective amplification coefficient of the gain in the combined system is $\alpha \approx -1.22 \times 10^4$ cm^{-1}, which is much larger than the amplification $\alpha \approx -9.2 \times 10^2$ cm^{-1} for the bulk gain material [14] at the given pumping rate $\Gamma_{\text{pump}} = 1.0 \times 10^9$ s^{-1}. This is due to the strong local electric field enhancement in the gap of the resonant SRR. While we have an incident electric field 10 V m^{-1}, the induced electric field in the gap is around 450 V m^{-1}. Taking the observed field enhancement factor around 45 in the gap of SRR, the energy produced by the gain in the gap is around 12 times larger than from the homogeneous bulk gain material in the size of the unit cell, which agrees well with the factor of around 15 between the simulated SRR effective medium and the homogeneous gain medium. If we continue

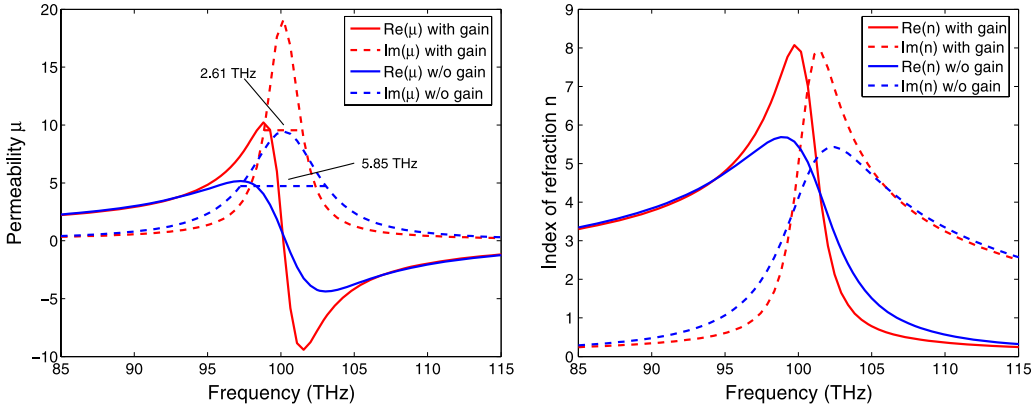

(a) (b)

Figure 18. The retrieved results for the real and the imaginary parts of (a) the effective permeability μ and (b) the corresponding effective index of refraction n, with and without gain for a pumping rate $\Gamma_{\text{pump}} = 1.0 \times 10^9$ s^{-1} and the SRR system of figure 17. The gain bandwidth is 20 THz. Notice that the width of the magnetic resonance with gain is 2.61 THz.

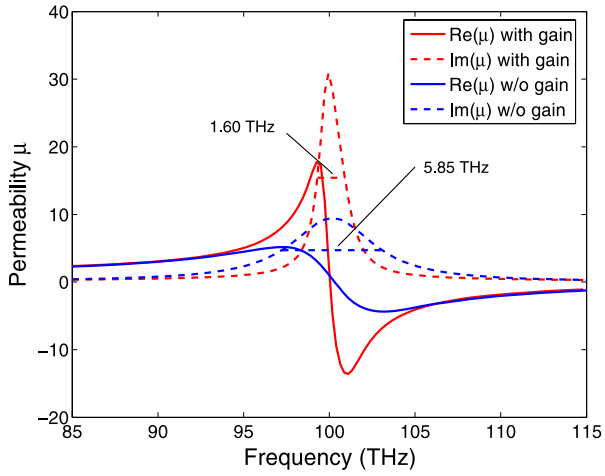

Figure 19. The retrieved results for the real and the imaginary parts of the effective permeability, μ, with and without gain for a pumping rate $\Gamma_{\text{pump}} = 8.0 \times 10^8\ \text{s}^{-1}$ and the SRR system where the SRR is surrounded by gain. The gain bandwidth is 20 THz. Notice that the width of the magnetic resonance with gain is 1.60 THz, narrower than figure 18(a).

increasing the pumping rate, the magnetic resonance becomes narrower (0.96 THz for pumping rate $\Gamma_{\text{pump}} = 1.8 \times 10^9\ \text{s}^{-1}$). When the pumping rate reaches $\Gamma_{\text{pump}} = 1.9 \times 10^9\ \text{s}^{-1}$, the metamaterial system gets overcompensated and the imaginary part of the effective permeability μ at the resonance frequency gets flipped down and becomes negative. If we increase the pumping rate even more (around $\Gamma_{\text{pump}} = 5.0 \times 10^9\ \text{s}^{-1}$), the SRR system starts lasing [21, 22].

Instead of having the gain in the gap of the SRR, we also have done simulations on the SRR system where the gain surrounds the SRR. The retrieved results for the real and the imaginary parts of the effective permeability μ without gain and with gain for a given pumping rate $\Gamma_{\text{pump}} = 8.0 \times 10^8\ \text{s}^{-1}$ are plotted in figure 19. Due to the larger gain filling in the unit cell, the coupling between the gain material and the SRR gets stronger and the losses of SRR are easier to compensate. Compared with the case with the gain in the gap only, the effective permeability μ, of the simulated SRR system in figure 19 has a stronger and narrower resonance (FWHM = 1.6 THz) even with a lower pumping rate. Similar to the previous case, the magnetic resonance becomes stronger and narrower (0.7 THz at $\Gamma_{\text{pump}} = 1.0 \times 10^9\ \text{s}^{-1}$) as we increase the pumping rate, and the system gets overcompensated so that the magnetic resonance peak gets flipped down when the pumping rate reaches $\Gamma_{\text{pump}} = 1.1 \times 10^9\ \text{s}^{-1}$. It is also easier for this system to have lasing [21, 22], which is observed when the pumping rate is $\approx \Gamma_{\text{pump}} = 2.5 \times 10^9\ \text{s}^{-1}$.

4. Conclusions

We have performed numerical simulations on a one-dimensional gain material system by using the FDTD method. The system starts lasing when the input exceeds the lasing threshold. For a greater input power and wider gain slab, the lasing is faster. Comparisons were done for a gain material slab between the optical pump method and its homogeneous pumping rate simplification and results show that this simplification can be valid for a thin gain slab.

A self-consistent model incorporating the gain into a dispersive metamaterial nanostructure was proposed and numerically solved. We numerically show that the losses of dispersive metamaterials can be compensated by gain by investigating the transmission, reflection and absorption data as well as the retrieved effective parameters. There is a relatively wide range of input signal amplitudes where the metamaterial–gain system behaves linearly. When the amplitudes get higher, the system becomes nonlinear, due to the nonlinearity of the gain material itself. It is necessary to have self-consistent calculations to determine the signal range where we can expect a linear response. Further, if we have strong signals, so that we are in nonlinear regime, or we want to study lasing, self-consistent calculation is needed. As examples, two SRR systems with different gain inclusions were studied. We have demonstrated that the magnetic losses of the SRRs can be easily compensated by the electric gain. The pumping rate needed to compensate the losses is much smaller than the bulk gain material. The losses of the SRR surrounded by gain can more easily be compensated than the SRR with gain in the gap, due to more coupling with the gain. Provided that the pumping rate is high enough, metamaterial nanostructures can lase.

Acknowledgments

Work at Ames Laboratory was supported by the Department of Energy (Basic Energy Sciences) under Contract No. DE-AC02-07CH11358. This work was partially supported by the Office of Naval Research (Award No. N00014-07-1-0359), by the Laboratory Directed Research and Development program at Sandia National Laboratories and BioTechnology group from AFRL/RXB.

Appendix. The FDTD algorithm for 2D TE modes

The FDTD algorithm is based on the straightforward spatially and temporally isotropic discretizations of Maxwell equations (Yee cell [15]) and the auxiliary equations for dispersive polarizations, gain oscillators and occupation numbers. Below, we show the relevant case of 2D TE modes (only E_z, H_x and H_y present) in dispersive Lorentz media and four-level gain materials. The algorithm for 2D TM modes is analogous to that for TE modes with H_z, E_x and E_y substituted for E_z, H_x and H_y and analogous for currents and polarizations.

For a lossy Lorentz media with the dispersive permittivity

$$\varepsilon(\omega) = 1 + \frac{\omega_{ep}^2}{\omega_p^2 - \mathrm{i}\omega\Gamma - \omega^2}, \tag{A.1}$$

we have

$$\frac{\mathbf{P}(\omega)}{\mathbf{E}(\omega)} = \frac{\varepsilon_0 \omega_{ep}^2}{\omega_p^2 - \mathrm{i}\omega\Gamma - \omega^2}. \tag{A.2}$$

By taking an inverse Fourier transform on (A.2) [15, 18], we can obtain the time-domain electric polarization equation for

the Lorentz media as follows:

$$\frac{\mathrm{d}^2\mathbf{P}(t)}{\mathrm{d}t^2}+\Gamma\frac{\mathrm{d}\mathbf{P}(t)}{\mathrm{d}t}+\omega_p^2\mathbf{P}(t)=\varepsilon_0\omega_{ep}^2\mathbf{E}(t). \tag{A.3}$$

Based on (A.3) and all the equations in section 2, we do the updates on magnetic fields H_x and H_y, electric polarization P_z and electric polarization current J_z ($\partial P_z/\partial t$), electric field E_z and the occupation numbers N_0–N_3.

For magnetic fields, both the Lorentz media and the gain materials have the same FDTD update algorithm as follows:

$$H_x^{l+\frac{1}{2}}(i,j+\tfrac{1}{2})=H_x^{l-\frac{1}{2}}(i,j+\tfrac{1}{2})-\frac{\Delta t}{\mu_0\Delta y}[E_z^l(i,j+1)-E_z^l(i,j)], \tag{A.4}$$

$$H_y^{l+\frac{1}{2}}(i+\tfrac{1}{2},j)=H_y^{l-\frac{1}{2}}(i+\tfrac{1}{2},j)+\frac{\Delta t}{\mu_0\Delta x}[E_z^l(i+1,j)-E_z^l(i,j)]. \tag{A.5}$$

The upper indices are time coordinates and the indices in parenthesis are spatial coordinates of the discretized fields.

For the Lorentz media, we have the update algorithm for P_z from the discretization of (A.3),

$$P_z^{l+1}(i,j)=\frac{2-\omega_p^2(\Delta t)^2}{1+\Gamma\Delta t/2}P_z^l(i,j)-\frac{1-\Gamma\Delta t/2}{1+\Gamma\Delta t/2}P_z^{l-1}(i,j)+\frac{\varepsilon_0\omega_{ep}^2(\Delta t)^2}{1+\Gamma\Delta t/2}E_z^l(i,j). \tag{A.6}$$

We have to store P_z for two time-steps in the FDTD update. For Drude metals, it is just a special case of the Lorentz media with the resonance frequency $\omega_p=0$. Also (A.3) can be simplified as a first-order derivative equation by taking $\omega_p=0$ and $J_z=\partial P_z/\partial t$, which brings us an advantage that we directly get J_z and only need to store J_z for one time-step.

For the optically pumped gain materials, we have the FDTD update algorithms for electric polarizations from the electric polarization equation (2):

$$P_{a,z}^{l+1}(i,j)=\frac{2-\omega_a^2\Delta t^2}{1+\Gamma_a\Delta t/2}P_{a,z}^l(i,j)-\frac{1-\Gamma_a\Delta t/2}{1+\Gamma_a\Delta t/2}P_{a,z}^{l-1}(i,j)+\frac{\sigma_a\Delta t^2}{1+\Gamma_a\Delta t/2}[N_1^l(i,j)-N_2^l(i,j)]E_z^l(i,j), \tag{A.7}$$

$$P_{b,z}^{l+1}(i,j)=\frac{2-\omega_b^2\Delta t^2}{1+\Gamma_b\Delta t/2}P_{b,z}^l(i,j)-\frac{1-\Gamma_b\Delta t/2}{1+\Gamma_b\Delta t/2}P_{b,z}^{l-1}(i,j)+\frac{\sigma_b\Delta t^2}{1+\Gamma_b\Delta t/2}[N_0^l(i,j)-N_3^l(i,j)]E_z^l(i,j), \tag{A.8}$$

$$P_z{}^{l+1}(i,j)=P_{a,z}^{l+1}(i,j)+P_{b,z}^{l+1}(i,j). \tag{A.9}$$

For the electric polarization current J_z and electric field E_z, the Lorentz media and the gain materials also have the same FDTD update algorithms,

$$J_z^{l+1/2}(i,j)=[P_z^{l+1}(i,j)-P_z^l(i,j)]/\Delta t, \tag{A.10}$$

$$E_z^{l+1}(i,j)=E_z^l(i,j)+\frac{\Delta t}{\varepsilon\varepsilon_0\Delta x}\left[H_y^{l+\frac{1}{2}}\left(i+\frac{1}{2},j\right)-H_y^{l+\frac{1}{2}}\left(i-\frac{1}{2},j\right)\right]-\frac{\Delta t}{\varepsilon\varepsilon_0\Delta y}\left[H_x^{l+\frac{1}{2}}\left(i,j+\frac{1}{2}\right)-H_x^{l+\frac{1}{2}}\left(i,j-\frac{1}{2}\right)\right]-\frac{J_z^{l+1/2}(i,j)}{\varepsilon\varepsilon_0}\Delta t, \tag{A.11}$$

where $\varepsilon=1$ for Lorentz media and the background dielectric constant for gain materials.

From the rate equations (3*a*)–(3*d*), we obtain the occupation-number FDTD algorithms for the optically pumped gain materials:

$$N_3^{l+1}(i,j)=\frac{1-\Delta t/2\tau_{32}}{1+\Delta t/2\tau_{32}}N_3^l(i,j)+\frac{1}{2\hbar\omega_b}\frac{1}{1+\Delta t/2\tau_{32}}\times[E_z^{l+1}(i,j)+E_z^l(i,j)]\times[P_{b,z}^{l+1}(i,j)-P_{b,z}^l(i,j)] \tag{A.12}$$

$$N_2^{l+1}(i,j)=\frac{1-\Delta t/2\tau_{21}}{1+\Delta t/2\tau_{21}}N_2^l(i,j)+\frac{1}{2\hbar\omega_a}\frac{1}{1+\Delta t/2\tau_{21}}\times[E_z^{l+1}(i,j)+E_z^l(i,j)][P_{a,z}^{l+1}(i,j)-P_{a,z}^l(i,j)]+\frac{1}{1+\Delta t/2\tau_{21}}\frac{\Delta t}{2\tau_{32}}[N_3^{l+1}(i,j)+N_3^l(i,j)] \tag{A.13}$$

$$N_1^{l+1}(i,j)=\frac{1-\Delta t/2\tau_{10}}{1+\Delta t/2\tau_{10}}N_1^l(i,j)-\frac{1}{2\hbar\omega_a}\frac{1}{1+\Delta t/2\tau_{10}}\times[E_z^{l+1}(i,j)+E_z^l(i,j)][P_{a,z}^{l+1}(i,j)-P_{a,z}^l(i,j)]+\frac{1}{1+\Delta t/2\tau_{10}}\frac{\Delta t}{2\tau_{21}}[N_2^{l+1}(i,j)+N_2^l(i,j)] \tag{A.14}$$

$$N_0^{l+1}(i,j)=N_0^l(i,j)-\frac{1}{2\hbar\omega_b}[E_z^{l+1}(i,j)+E_z^l(i,j)]\times[P_{b,z}^{l+1}(i,j)-P_{b,z}^l(i,j)]+\frac{\Delta t}{2\tau_{10}}[N_1^{l+1}(i,j)+N_1^l(i,j)]. \tag{A.15}$$

For gain materials using a constant pumping rate Γ_{pump}, we simply omit the update for the electric polarization $P_{b,z}$ on the atomic transition between N_0 and N_3 and use a constant pumping rate Γ_{pump} in the FDTD update algorithms for N_0 and N_3.

References

[1] Shalaev V M 2007 *Nat. Photon.* **1** 41
[2] Soukoulis C M, Linden S and Wegener M 2007 *Science* **315** 47
[3] Pendry J B 2000 *Phys. Rev. Lett.* **85** 3966
[4] Schurig D, Mock J J, Justice B J, Cummer S A, Pendry J B, Starr A F and Smith D R 2006 *Science* **314** 977
[5] Leonhardt U 2006 *Science* **312** 1777
[6] Zharov A A, Shadrivov I V and Kivshar Y S 2003 *Phys. Rev. Lett.* **91** 037401
O'Brien S, McPeake D, Ramakrishna S A and Pendry J B 2004 *Phys. Rev.* B **69** 241101
[7] Dolling G, Enkrich C, Wegener M, Soukoulis C M and Linden S 2006 *Opt. Lett.* **31** 1800
[8] Govyadinov A A, Podolskiy V A and Noginov M A 2007 *Appl. Phys. Lett.* **91** 191103
[9] Gordon J A and Ziolkowski R W 2008 *Opt. Express* **16** 6692
[10] Ramakrishna S A and Pendry J B 2003 *Phys. Rev.* B **67** 201101
[11] Lawandy N M 2004 *Appl. Phys. Lett.* **85** 5040
[12] Klar T A, Kildishev A V, Drachev V P and Shalaev V M 2006 *IEEE J. Sel. Top. Quantum Electron.* **12** 1106
[13] Wegener M, García-Pomar J L, Soukoulis C M, Meinzer N, Ruther M and Linden S 2008 *Opt. Express* **16** 19785
[14] Siegman A E 1986 *Lasers* (Mill Valley, CA: University Science Books) chapters 2, 3, 6, and 13
[15] Taflove A 1995 *Computational Electrodynamics: The Finite Difference Time Domain Method* (London: Artech House Publishers) chapters 3, 6, 7
[16] Jiang X and Soukoulis C M 2000 *Phys. Rev. Lett.* **85** 70

[17] Bermel P, Lidorikis E, Fink Y and Joannopoulos J D 2006 *Phys. Rev.* B **73** 165125
[18] Joseph R M, Hagness S C and Taflove A 1991 *Opt. Lett.* **16** 1412
[19] Ziolkowski R W, Arnold J M and Gogny D M 1995 *Phys. Rev.* A **52** 3082
[20] Smith D R, Schultz S, Markoš P and Soukoulis C M 2002 *Phys. Rev.* B **65** 195104
[21] Bergman D J and Stockman M I 2003 *Phys. Rev. Lett.* **90** 027402
[22] Zheludev N I, Prosvirnin S L, Papasimakis N and Fedotov V A 2008 *Nat. Photon.* **2** 351